

## The Gamma-ray Activity of the high-z Quasar 0836+71

Svetlana Jorstad<sup>1,2,a</sup>, Alan Marscher<sup>1</sup>, Valeri Larionov<sup>2</sup>, José L. Gómez<sup>3</sup>, Iván Agudo<sup>3,1,4</sup>, Emmanouil Angelakis<sup>5</sup>, Carolina Casadio<sup>3</sup>, Mark Gurwell<sup>6</sup>, Talvikki Hovatta<sup>7</sup>, Manasvita Joshi<sup>1</sup>, Lars Fuhrmann<sup>5</sup>, Vassilis Karamanavis<sup>5</sup>, Anne Lähteenmäki<sup>8</sup>, Sol Molina<sup>3</sup>, Daria Morozova<sup>2</sup>, Ioannis Myserlis<sup>5</sup>, Ivan Troitsky<sup>2</sup>, Hans Ungerechts<sup>9</sup>, and J. Anton Zensus<sup>5</sup>

<sup>1</sup>*Institute for Astrophysical Research, Boston University, Boston, MA, USA*

<sup>2</sup>*St. Petersburg State University, St. Petersburg, Russia*

<sup>3</sup>*Instituto de Astrofísica de Andalucía, Granada, Spain*

<sup>4</sup>*Joint Institute for VLBI in Europe, Dwingeloo, the Netherlands*

<sup>5</sup>*Max-Plank-Institut für Radioastronomie, Bonn, Germany*

<sup>6</sup>*Harvard-Smithsonian Center for Astrophysics, Cambridge, MA, USA*

<sup>7</sup>*California Institute of Technology, Pasadena, CA, USA*

<sup>8</sup>*Aalto University Metsähovi Radio Observatory, Kylmälä, Finland*

<sup>9</sup>*Instituto de Radioastronomía Milimétrica (IRAM), Granada, Spain*

**Abstract.** The Fermi LAT detected an increase in  $\gamma$ -ray activity of the quasar 0836+710 ( $z=2.17$ ) in Spring 2011 that culminated in a sharp  $\gamma$ -ray flare at the end of 2011 when the source reached a flux of  $2.9 \times 10^{-6}$  phot  $s^{-1}cm^{-2}$  at 0.1-200 GeV. We monitor the quasar at optical wavelengths in photometric and polarimetric modes, at millimeter and centimeter wavelengths, and with the VLBA at 43 GHz. The optical brightness of the quasar increased by  $\sim 0.5$  mag in  $R$  band and the degree of polarization oscillated between  $\sim 1\%$  and  $\sim 6\%$  during the highest  $\gamma$ -ray state, while the position angle of polarization rotated by  $\sim 300^\circ$ . We have identified in the VLBA images a strong, highly polarized component that moves with an apparent speed of  $\sim 20 c$ . The component emerged from the core in the beginning of the  $\gamma$ -ray event and reached a flux maximum at the peak of the  $\gamma$ -ray outburst. We present the results of a correlative analysis of variations at different wavelengths along with the kinematic parameters of the parsec scale jet. We discuss the location of the high  $\gamma$ -ray emission in the relativistic jet, as well as the emission mechanisms responsible for  $\gamma$ -ray production.

## 1 Introduction

The quasar 0836+71 (4C+71.7) is the most distant source at  $z=2.172$  [1] among the  $\gamma$ -ray blazars which Boston University group monitors with the Very Long Baseline Array (VLBA) at 43 GHz<sup>1</sup>. Kaspi et al. [2] have measured a tentative rest-frame delay of  $\sim 188$  days between variations of the *UV* continuum and *CIV* emission line of 0836+71 and estimated the black hole mass (BH) of  $\sim 2.6 \times 10^9 M_\odot$ . The bolometric luminosity of  $3.6 \times 10^{47}$  erg  $s^{-1}$  then suggests that the BH is accreting close to its Eddington luminosity. The quasar has a highly relativistic jet with apparent speeds up to  $21c$  [3]. It was identified as a  $\gamma$ -ray source by the *Energetic Gamma-Ray Experiment Telescope* [4]. Although the quasar is listed in the First and Second Catalogs (J0841.6+7052) produced by the *Fermi* Large Area Telescope (LAT) team [5, 6], it was fairly quiet during the first two years of the *Fermi* LAT operations with an average  $\gamma$ -ray flux of  $S = (1.8 \pm 0.7) \times 10^{-8}$  phot  $s^{-1}cm^{-2}$  at  $E > 100$  MeV. However, in March 2011 the blazar underwent an increase in  $\gamma$ -ray emission. The  $\gamma$ -ray ac-

tivity lasted for a year, culminating on November 1st, 2011 when the  $\gamma$ -ray flux reached a maximum of  $S_\gamma = (2.9 \pm 0.4) \times 10^{-6}$  phot  $s^{-1}cm^{-2}$  at  $E > 100$  MeV, which corresponds to a luminosity of  $(1.1 \pm 0.2) \times 10^{49}$  erg  $s^{-1}$  ( $H_\odot = 71$  km  $s^{-1}Mpc^{-1}$ ,  $\Omega_m = 0.27$ ,  $\Omega_\Lambda = 0.73$ ). The multi-frequency behavior of 0836+71 during the  $\gamma$ -ray-outburst has been discussed by Akyuz et al. [7]. These authors find a significant change of the shape of the  $\gamma$ -ray spectrum from straight to curved in the  $\log S_\gamma - \log v$  plane, evidence for a positive correlation between  $\gamma$ -ray and optical flaring emission, and no clear correlation between  $\gamma$ -ray and radio variations. Since 2007 June we have been observing 0836+71 with the VLBA at 43 GHz roughly monthly and performing optical measurements in photometric and polarimetric modes as frequently as the telescopes' schedule and weather allow. Here we present analysis of both the multi-frequency light curves of 0836+71 and parsec-scale jet behavior during and after the prominent  $\gamma$ -ray event.

## 2 Observations and Data Reduction

We have constructed the  $\gamma$ -ray light curve at energies from 100 MeV to 200 GeV with a bin size of one week from

<sup>a</sup>e-mail: jorstad@bu.edu

<sup>1</sup><http://www.bu.edu/blazars/VLBAproject.html>

the beginning of the *Fermi* mission up to 2013 May using *Pass 7* photon and spacecraft data, version *V9r23p1* of the *Fermi* Science Tools, and the instrument responses for the *gal\_2yearp7v6\_v0* and *iso\_p7v6clean.txt* diffuse source models. We have also computed the fluxes with a bin size of 3 days over the period from 2011 February 25 to 2012 March 25 and with a bin size of 1 day for the brightest  $\gamma$ -ray state from 2011 October 25 to 2012 January 5. We have used a power-law model with the photon index  $\alpha_\gamma = 2.95$  as listed in the 2FGL catalog [6] during quiescent periods, and allow  $\alpha_\gamma$  to vary in calculations during the active state.

We observed 0836+71 with *RXTE* at 2.4-10 KeV twice per week from 2009 February 6 to 2010 February 10 and with the *Suzaku* XIS at 0.2-15 KeV on 2012 October 13. We have downloaded the data from the *Swift* archive, which contains sporadic measurements with the *Swift* XRT at 0.2-10 KeV from 2006 April 1 to 2012 April 3. The X-ray data were reduced using the standard *HEAsoft* package (version 6.11). We fit the spectra in *xspec* using a power-law model with the hydrogen column density  $N_H = 2.9 \times 10^{20} \text{ cm}^{-2}$  [8].

The optical photometric data were obtained at various telescopes: 1) the 1.83 m Perkins telescope of Lowell Observatory (Flagstaff, AZ), 2) the 70 cm AZT-8 telescope of the Crimean Astrophysical Observatory (Nauchnij, Ukraine); 3) the 40-cm LX-200 telescope of St. Petersburg State University (St. Petersburg, Russia); 4) the 2.2 m telescope of Calar Alto Observatory (Almería, Spain); 5) the 2 m Liverpool telescope of the Observatorio del Roque de Los Muchachos (Canary Island, Spain); and 6) the *Swift* UVOT. At telescopes 1-3 measurements were performed in BVRI bands, at telescopes 4-5 in R band, and at the UVOT in BV bands plus four UV filters. The optical polarization observations were carried out at telescopes 1-4 in R band, except the LX-200 telescope, where the linear polarization were measured without a filter, with a central wavelength at  $\lambda_{\text{eff}} \sim 670 \text{ nm}$ .

We use radio measurements obtained at 1) the Sub-Millimeter Array (SMA, Mauna Kea, Hawaii) at 1.3 mm (230 GHz), 2) the 30-meter IRAM telescope (Pico Veleta, Spain) at 1.3 mm, 2 mm (142 GHz), and 3 mm (86 GHz); 3) the 13.7 m telescope at Metsähovi Radio Observatory (Aalto University, Finland) at 8 mm (37 GHz), and 4) the 40 m telescope at the Owens Valley Radio Observatory (OVRO) at 2 cm (15 GHz).

The multi-wavelength light curves of the quasar are presented in Figure 1. The curves of optical polarization parameters along with the  $\gamma$ -ray and optical light curves are given in Figure 2.

We have obtained total and polarized intensity images of 0836+71 at 19 epochs with the VLBA at 43 GHz from 2011 March to 2013 January. The VLBA data were calibrated and imaged in a manner identical to that described in [9]. We modelled the images in terms of a small number of components with circular Gaussian brightness distributions and determine polarization parameters of components using an IDL program that calculates the mean

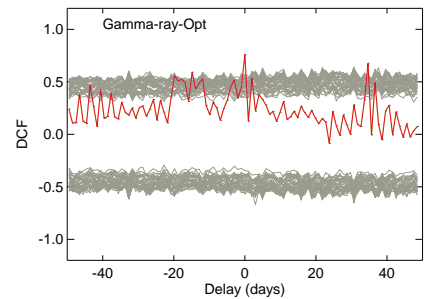


**Figure 3.** Discrete cross-correlation function (DCF) between the  $\gamma$ -ray and optical light curves (the red curve). The gray curves define a level of significance  $\sim 99.7\%$  based on DCF computations involving 3000 simulated light curves.

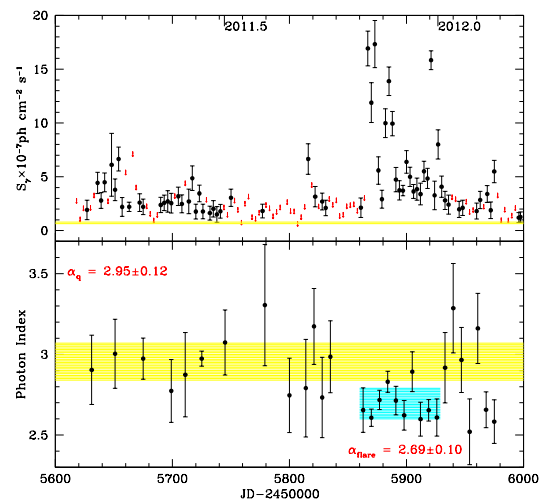


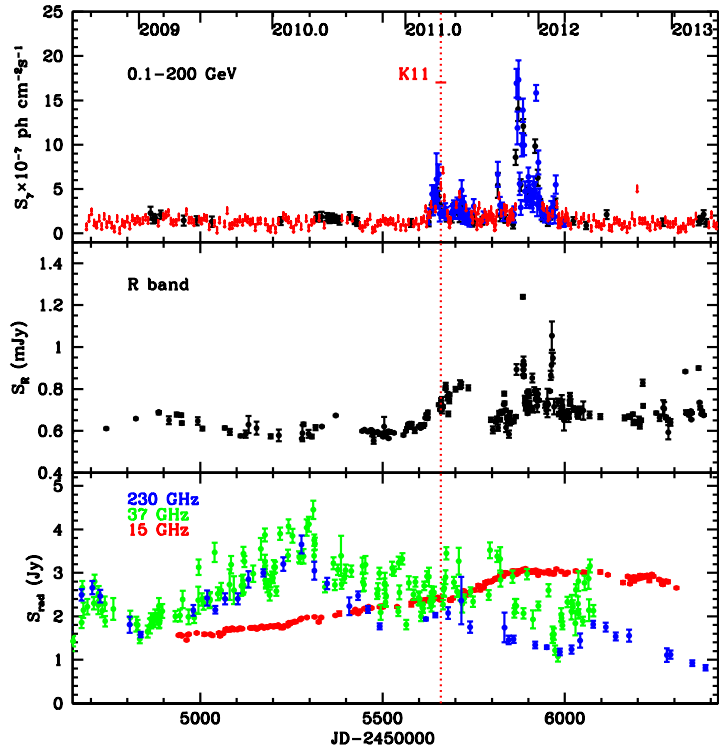
**Figure 4.** *Top:*  $\gamma$ -ray light curve during the high  $\gamma$ -ray state, the yellow horizontal line marks a quiescent flux level. *Bottom:*  $\gamma$ -ray photon index vs. time, the yellow area shows a typical photon index of 0836+71, the blue area shows the most probable  $\alpha_\gamma$  values during the brightest  $\gamma$ -ray state.

values within an area equal to that of the size established by the model fit.

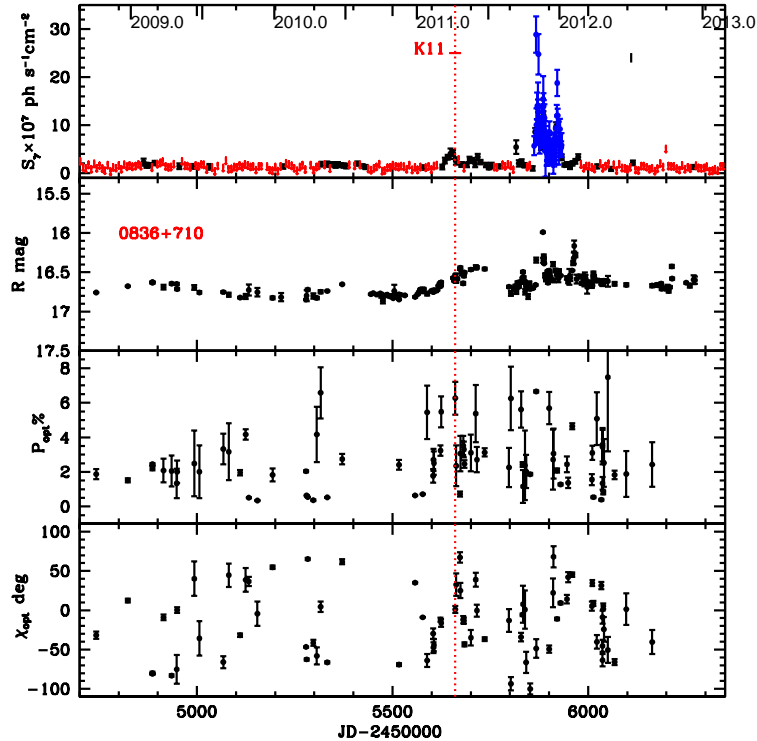
### 3 Variability at Different Wavelengths

Figure 1 shows that the  $\gamma$ -ray outburst has a counterpart at the optical wavelengths with similar structure and duration. The cross-correlation analysis between the light curves (Figure 3), performed in the same manner as described in [10], suggests that there is a statistically significant positive correlation between  $\gamma$ -ray and optical variations without any delay  $> 1$  day. Figure 4 shows variations of the photon index during the high  $\gamma$ -ray state. In the beginning of the event  $\alpha_\gamma$  did not deviate significantly from that given in the 2FGL catalog, while during the brightest  $\gamma$ -ray state a flattening of the photon index is apparent at the  $2.5\sigma$  significance level.

Figure 5 shows measurements at X-rays energies along with the photon index,  $\alpha_X$ . Although the X-ray light curve



**Figure 1.** Light curves of the quasar 0836+71. From the top:  $\gamma$ -ray light curve, red arrows designate upper limits, blue points correspond to the flux densities calculated with a bin size of three days; optical light curve, and radio light curves at 15 GHz (red), 37 GHz (green), and 86 GHz (blue); the vertical dotted red line marks the time of passage of *K11* through the core.



**Figure 2.** From the top:  $\gamma$ -ray light curve (blue points correspond to the flux densities calculated with a bin size of one day), optical light curve, degree of optical polarization, and position angle of optical polarization for 0836+71; the vertical dotted red line marks the time of passage of *K11* through the core.

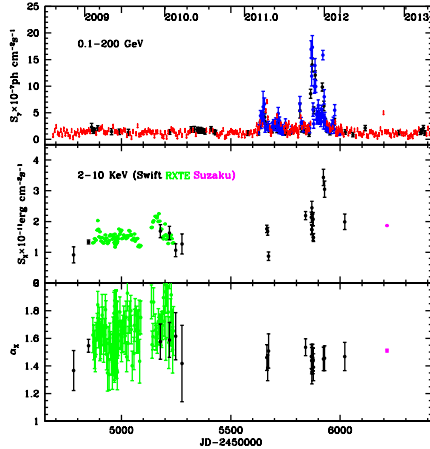


**Figure 5.** Top:  $\gamma$ -ray light curve during of 0836+71. Middle: X-ray light curve. Bottom: X-ray photon index vs. time.

**Table 1.** Parameters of Variability

Frequency	$\tau_{var}$ day	$T_{max}$ MJD	$S_{max}$ erg $s^{-1}cm^{-2}Hz^{-1}$
1 GeV	0.4	55866.547	$(7.53 \pm 1.21) \times 10^{-34}$
1 keV	0.8	55922.986	$(2.58 \pm 0.20) \times 10^{-29}$
670 nm	2.3	55884.065	$(1.23 \pm 0.01) \times 10^{-26}$

is sparse, an increase of the flux in Autumn 2011 is clearly visible and, perhaps, simultaneous with the  $\gamma$ -ray event. The X-ray photon index is significantly flatter than  $\alpha_\gamma$ . Despite large uncertainties of  $\alpha_X$ , especially during a quiescent period, a tentative flattening of  $\alpha_X$  from  $\sim 1.6$  during the quiescent period to  $\sim 1.5$  during the outburst is indicated. We have analyzed the timescale and amplitude of flux variability from  $\gamma$ -rays to optical wavelengths during the high  $\gamma$ -ray state. We have determined a minimum time scale of the variability,  $\tau_{var}$ , the epoch of the peak and peak flux density of the outburst at each wavelength,  $T_{max}$  and  $S_{max}$ , respectively, and the factor  $f$  of the flux increase during the peak with respect to the average quiescent flux level (Table 1). The value of  $\tau_{var}$  is equal to the minimum time interval in the light curve required for doubling of the flux at a given frequency. The  $\gamma$ -ray flux shows the shortest timescale and largest amplitude of variability with respect to longer wavelengths, as observed for other blazars as well [e.g., 11]. However, the amplitude of variability at optical wavelengths is most likely masked by a contribution from the thermal emission of the accretion disk. This is supported by a reddening of the source when it becomes brighter, and by a low degree of the optical polarization during quiescent states (see below). Akyuz et al. [7] have estimated the contribution from the accretion disk in R band to be  $\sim 0.55$  mJy and computed an amplitude of variability of the optical synchrotron component of  $\sim 7$ . The X-ray light curve of 0836+71 also suggests the presence of a steady component that dominates the X-ray quiescent emission. Although the global  $\gamma$ -ray peak coincides neither with the X-ray nor optical maximum, this can be explained by sparser sampling of the X-ray and optical

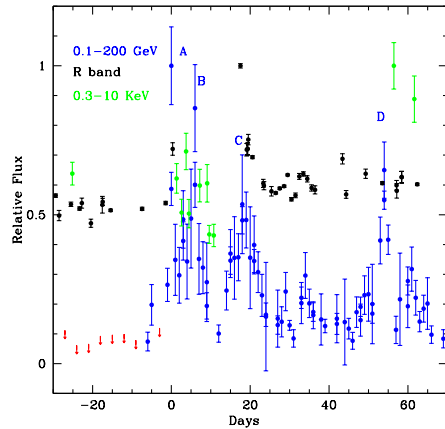


**Figure 6.** Relative flux at  $\gamma$ -ray (blue), X-ray (green), and optical (black) wavelengths vs. time with respect to  $T_{max}$  of the  $\gamma$ -ray outburst.

light curves. On the other hand, the  $\gamma$ -ray outburst has several peaks (marked in Figure 6 as A, B, C, and D), relative amplitudes of which seem to vary across wavelengths in a different manner while the structure of the outburst is perhaps roughly similar. Such behavior could be connected with an interplay between the synchrotron self-Compton (SSC) and external inverse Compton (EC) mechanisms for high energy production caused by variations in the density of the seed photon field and strength of the magnetic field (e.g., [12]). The latter would imply that the  $\gamma$ -ray flares A, B, C, and D originate in different places or in a moving emission region.

The radio light curves at short wavelengths ( $\leq 8$  mm) show an outburst that started  $\sim 1.5$  yr earlier than the  $\gamma$ -ray event (Figure 1). Although there is activity at mm wavelengths during the  $\gamma$ -ray outburst and the flux at 15 GHz reaches a maximum in the form of a plateau with a duration of several months that peaks at the maximum of the  $\gamma$ -ray outburst, the connection between  $\gamma$ -ray and radio light curves is not clear, as discussed by Akyuz et al. [7].

#### 4 Jet Kinematics

The parsec-scale jet of the quasar 0836+71 is strongly core dominated at 43 GHz (Figure 7). We have constructed the light curve of the VLBI core, A0, which shows a good correlation with the mm-wave light curves from the whole source (Figure 8). The VLBA images reveal brightening of A0 that started in the second half of 2009 along with an increase of the flux in the mm-wave light curves. The global maximum at 86 GHz on 2010 March 22 (RJD:5278) appears to be contemporaneous with the brightest state of the core on 2010 March 6. The second (in amplitude) maximum of the core flux, reached on 2011 April 21 (RJD:5673), coincides with the second maximum of the 86 GHz light curve. The radio spectral index,  $\alpha_{rad}$ , calculated using 142, 86, and 37 GHz measurements, steepens as the mm-wave outburst evolves (Figure 8). Analysis of the parsec-scale jet behavior indicates that the second

maximum is associated with the appearance of a new superluminal knot,  $K11$ , in the jet (Figure 9).  $K11$  moves with apparent speed  $\beta_{app}=19.7\pm1.2$  c (Figure 10). Extrapolation of its motion back in time gives the epoch of the passage of the knot through the core to be around 2011 April 9,  $T_o = 2011.27\pm0.02$ . The trajectory of  $K11$  is ballistic in the projection on the plane of sky, which suggests that an apparent deceleration of the knot by a factor of  $\sim 2$  seen beyond  $\sim 0.2$  mas from the core (Figure 10) might be intrinsic. We used the method proposed by Jorstad et al. [9] to estimate the Doppler,  $\delta$ , and Lorentz,  $\Gamma$ , factors, and viewing angle,  $\Theta_o$ , of the jet. The method yields  $\delta \sim 21.3$ ,  $\Gamma \sim 19.8$ , and  $\Theta_o \sim 2.7^\circ$  within 0.2 mas from the core. Figure 10 also shows the light curve of  $K11$ , which peaks near the maximum of the  $\gamma$ -ray outburst. At this time a prominent outburst is seen in the 37 GHz light curve, while at shorter mm-wavelengths an increase of the flux is negligible, which yields the steepest value of  $\alpha_{rad}$  close to  $T_{max}^\gamma$  (Figure 8). The latter favors  $K11$  being responsible for the increase of the flux at mm wavelengths at this epoch, since the knot is most likely optically thin, with the spectral peak within  $\sim 10$ -50 GHz.

The absence of a disturbance downstream of the core, which can be associated with the global maximum at mm wavelengths, is puzzling. Neither the  $\gamma$ -ray nor optical light curves show a significant increase of the flux during this global peak at mm wavelengths, while the appearance of  $K11$  in the jet manifests the beginning of both the  $\gamma$ -ray and optical activity (Figures 1 & 2).

The parsec-scale jet of 0836+71 extends out to 3 mas at 43 GHz (1 mas=8.39 pc). A compact feature,  $C$ , is located at the south west end of the jet (Figure 7). The quasar is observed also within the MOJAVE<sup>2</sup> program at 15 GHz. One of the observations, on 2011 May 21, is very close to the epoch of our observations at 43 GHz (2011 May 22). This allows us to measure the difference between the positions of the core at 43 GHz and 15 GHz with respect to knot  $C$ , which is  $0.16\pm0.03$  mas. Using the value of the viewing angle derived above, we estimate that the VLBI core at 43 GHz lies closer to the BH than the 15 GHz core by  $\sim 28.5$  pc. According to a study by Pushkarev et al. [13], the core of 0836+71 at 15 GHz is located  $\sim 42.5$  pc from the BH. This suggests that the 43 GHz core is located  $\sim 14$  pc from the BH. If the enhanced  $\gamma$ -ray emission is associated with superluminal knot  $K11$ , as can be inferred from our analysis, the dissipation zone during the peak of the  $\gamma$ -ray outburst was located at a distance  $\sim 35$  pc from the BH.

## 5 Polarization Behavior

The quasar 0836+71 displays a moderate degree of optical polarization,  $P_{opt}$ , for a blazar, usually  $\sim 1$ -3% (Figure 2). The highest polarization, which has been observed since Summer 2008, is  $\sim 7\%$ . This suggests a significant contribution of the accretion disk in the optical emission

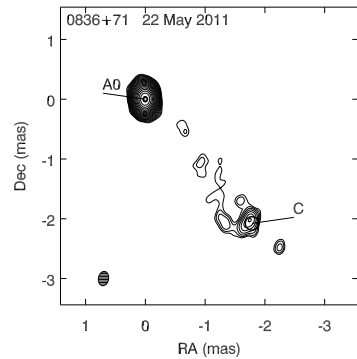


**Figure 7.** Total intensity image of 0836+71 at 43 GHz,  $S_{peak}=1.82$  Jy beam $^{-1}$  with a beam size of  $0.24\times0.17$  mas at PA= $-10^\circ$ .

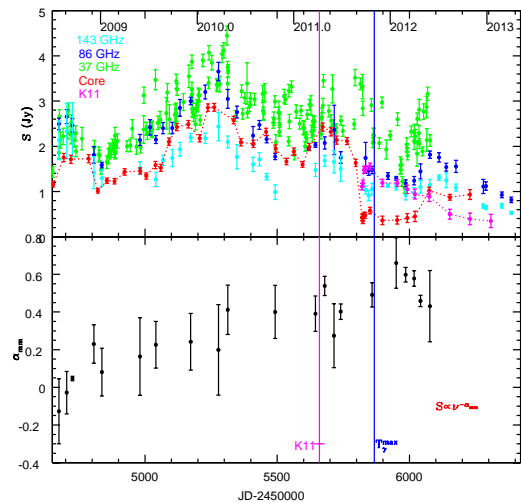


**Figure 8.** *Top:* Radio light curves at mm wavelengths and light curves of the VLBI core,  $A0$ , and knot  $K11$  (dotted red and magenta curves, respectively). *Bottom:* Evolution of mm wave radio spectral index  $\alpha_{rad}$ . The vertical magenta line shows the time of the passage of knot  $K11$  through the core, the vertical blue line marks the epoch of the maximum of the  $\gamma$ -ray flux.

of the quasar, especially during quiescent periods. Polarized emission at 43 GHz higher than a noise level is detected mainly in the core and/or a newly emerging knot (Figure 9). The degree of the radio polarization,  $P_{43}$ , does not exceed 3% (Figure 11). In general, there is no connection between  $P_{opt}$  and  $P_{43}$ . However, some interesting behavior of  $P_{opt}$  can be seen in Figure 2 that might be associated with the ejection of  $K11$ . Just before and several months after the appearance of  $K11$  in the jet, when  $K11$  was within 0.2 mas from the core and moved at its highest apparent speed, the degree of optical polarization oscillated between a very low  $P_{opt} \sim 1\%$  and  $P_{opt} \sim 6\%$ , displaying a kind of “see-saw” behavior, while outside this time interval  $P_{opt}$  varies more smoothly. A tighter connection between the optical polarization and polarization in the jet can be inferred from a comparison of variations of the position angle of optical polarization,  $\chi_{opt}$ , with that of polarization of  $K11$ ,  $\chi_{43}$ . Figure 2 shows that  $\chi_{opt}$  rotates during the period of “see-saw” behavior by several

<sup>2</sup>Monitoring Of Jets in Active galactic nuclei with VLBA Experiments, <https://www.physics.purdue.edu/astro/mojave/>

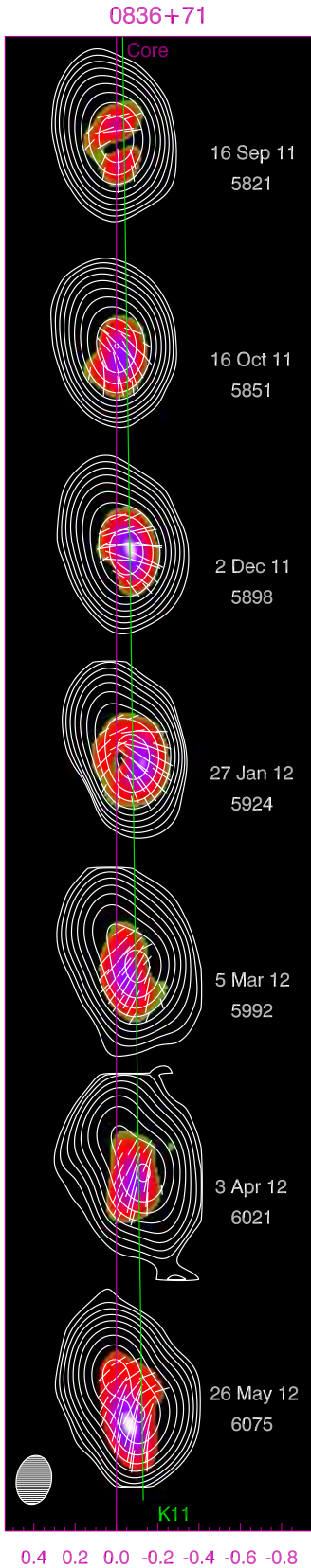


**Figure 9.** Total (contours) and polarized (color scale) intensity images of 0836+71 at 43 GHz with  $S_{peak}=1.37$  Jy beam $^{-1}$ ,  $S_{peak}^{pol}=30$  mJy beam $^{-1}$ , and beam size of  $0.24\times 0.17$  mas at PA=−10°. Line segments within the image show direction of linear polarization, the vertical magenta line marks the position of the core across epochs, while the green vertical line shows the evolution of knot K11.

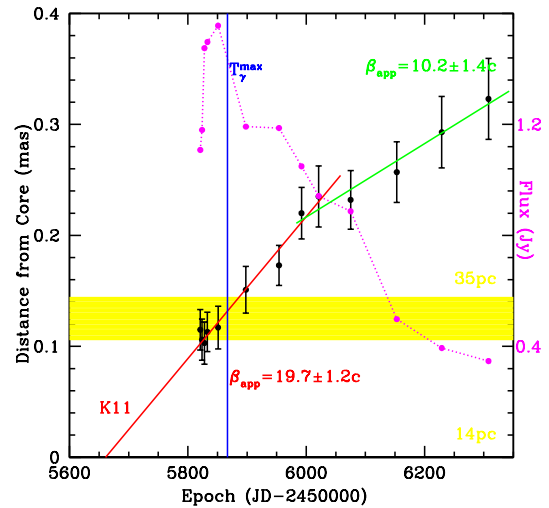


**Figure 10.** Separation of K11 from the core (black filled circles) as a function of time and the light curve of K11 (magenta filled circles connected by the dotted curve). The vertical blue line indicates the epoch of the peak of the  $\gamma$ -ray outburst, while the yellow area marks a location in the jet of the high energy dissipation zone during the  $\gamma$ -ray peak.

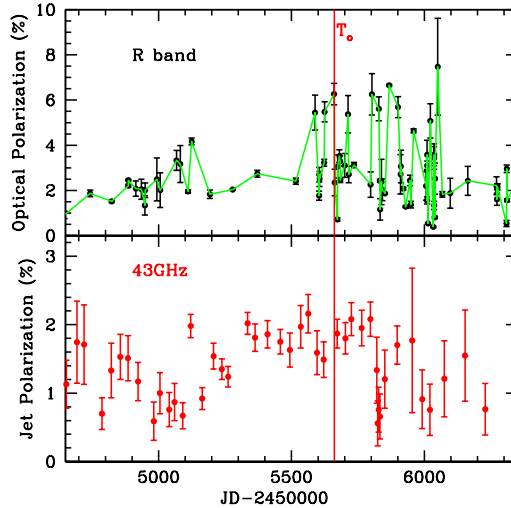


**Figure 11.** Top: Degree of optical polarization vs. time. Bottom: Degree of radio polarization integrated over the jet at 43 GHz. The red vertical line shows the time of passage of K11 through the core.

180° cycles. The rotation starts right at the beginning of the  $\gamma$ -ray activity, coincident with the ejection of K11. Rotation of  $\chi_{43}$  is also clearly visible in Figure 9. Although comparison of the two, displayed in Figure 12, does not imply that  $\chi_{opt}=\chi_{43}$  at the same time, but it does reveal rotation of both position angles in the same manner. This favors that knot K11 is responsible for the optical flaring behavior, and, therefore, the  $\gamma$ -ray outburst. Larionov et al. [14] explain optical photometric and polarimetric behavior of the blazar 0716+71, in particular rotation of the position angle of optical polarization, within a model of a compact emission region moving along a spiral trajectory.

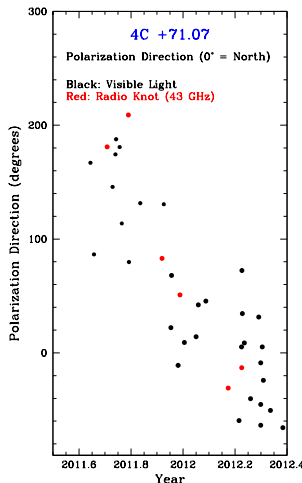


**Figure 12.** Position angle of polarization in optical R band (black filled circles) and of knot K11 (red filled circles) vs. time.

Although we cannot reject such a model, ballistic motion of  $K11$  and “see-saw” behavior of the degree of optical polarization are difficult to explain within that scenario. We propose a model, in which a rotating asymmetrical emission region with frozen magnetic field moves ballistically down the jet.

## 6 Conclusion

We have analyzed the multi-frequency light curves of the quasar 0836+716 along with the parsec-scale jet behavior in mm-wave VLBA images during and after the prominent  $\gamma$ -ray outburst. We summarize our findings as follows:

- The quasar 0836+71 had an active  $\gamma$ -ray state from 2011 March to 2012 March, with the highest  $\gamma$ -ray flux on 2011 November 1. The highest  $\gamma$ -ray state was accompanied by a flattening of the spectrum at 0.1-200 GeV in the case of a power-law model.
- The  $\gamma$ -ray and optical light curves show a statistically significant correlation without a measurable delay. A contemporaneous increase of the X-ray emission is observed as well.
- The start of the  $\gamma$ -ray activity coincides with the appearance of a superluminal knot in the parsec scale jet with  $\Gamma \sim 20$ . The peak of the  $\gamma$ -ray emission occurred during the brightest state of the knot according to the VLBA images and the behavior of the spectral index at mm wavelengths. The  $\gamma$ -ray outburst stopped as the knot decelerated to  $\Gamma \sim 12$ .
- The optical polarization behavior reveals a connection with properties of the innermost jet region when the knot was within 0.2 mas of the core.
- We connect the enhanced  $\gamma$ -ray emission with the superluminal knot propagating from the mm-wave core down

the jet and place the emission region of the highest  $\gamma$ -ray flux at  $\sim 35$  pc from the BH.

**This study, along with many others, demonstrates that continuation of operation of the VLBA is extremely important for our understanding of the physics of the most energetic objects in the Universe.**

## Acknowledgements

The VLBA is operated by the National Radio Astronomy Observatory. The National Radio Astronomy Observatory is a facility of the National Science Foundation, operated under cooperative agreement by Associated Universities, Inc. The Boston University group was partly funded by NASA Fermi Guest Investigator grants NNX11AQ03G, NNX11AO37G, and NNX12AO90G. The research at St. Petersburg State University was partly funded by RFBR grant 12-02-31193 and 12-02-00452. I. Agudo acknowledges funding support from the Spanish Ministry of Economy and Competitiveness and Regional Government of Andalucía grants AYA2010-14844 and P09-FQM-4784. The Liverpool Telescope is operated on the island of La Palma by Liverpool John Moores University in the Spanish Observatorio del Roque de los Muchachos of the Instituto de Astrofísica de Canarias, with funding from the UK Science and Technology Facilities Council. The Calar Alto Observatory is jointly operated by the Max-Planck-Institut für Astronomie and the Instituto de Astrofísica de Andalucía-CSIC. The OVRO 40-m monitoring program is supported in part by NASA grants NNX08AW31G and NNX11A043G, and NSF grants AST-0808050 and AST-1109911. The Submillimeter Array is a joint project between the Smithsonian Astrophysical Observatory and the Academia Sinica Institute of Astronomy and Astrophysics, and is funded by the Smithsonian Institution and the Academia Sinica. This work is also based on observations with the IRAM 30-m telescope.

## References

- [1] Stickel, M. & Kuehr, H., *A&ApS*, **100**, 395 (1993)
- [2] Kaspi, S., et al, *ApJ*, **659**, 997 (2007)
- [3] Lister, M., et al, *arXiv:1308.2731* (2013)
- [4] Hartman, R. C., et al, *ApJS*, **123**, 79 (2007)
- [5] Abdo, A. A., et al., *ApJS*, **188**, 405 (2010)
- [6] Nolan, P. L., et al., *ApJS*, **199**, 31 (2012)
- [7] Akyuz, A., et al., *A&Ap*, **556**, A71 (2013)
- [8] Kalberla, P. M. W., et al., *A&Ap*, **440**, 775 (2005)
- [9] Jorstad, S. G., et al. *AJ*, **130**, 1418 (2005)
- [10] Chatterjee, R., et al. *ApJ*, **689**, 79 (2008)
- [11] Jorstad, S. G., et al. *ApJ*, **773**, 147 (2013)
- [12] Marscher, A. P., et al., *ApJL*, **710**, L126 (2010)
- [13] Pushkarev, A. B., et al. *A&Ap*, **545**, A113 (2013)
- [14] Larionov, V. M., et al., *ApJ*, **768**, 40 (2013)